A quasi 3D approach for the modelling of an automotive turbocharger's compressor

G. Montenegro, M. Tamborski, A. Marinoni, A. Della Torre, A. Onorati, and S. Marelli

View Online   Export Citation

ARTICLES YOU MAY BE INTERESTED IN

A Quasi 3D Approach for the Modelling of an Automotive Turbocharger's Compressor

G.Montenegro[1,a)], M.Tamborski[1,b)], A.Marinoni[1,c)], A.Della Torre[1,d)], A.Onorati[1,e)], S.Marelli[2,f)]

[1]*Dipartimento di Energia, Politecnico di Milano, Milano, Italy*
[2]*Università degli Studi di Genova, Genoa, Italy*

a)gianluca.montenegro@polimi.it
b)matteo.tamborski@polimi.it
c)andreamassimo.marinoni@polimi.it
d)augusto.dellatorre@polimi.it
e)angelo.onorati@polimi.it
f)silvia.marelli@unige.it

Abstract. In this work the 3DCell method has been extended to the thermo-fluid dynamic simulation of an automotive turbocharger's compressor. The 3DCell, an approach continuously developed by the authors at Politecnico di Milano, is based on a pseudo-staggered leapfrog method that allows to decompose a generic 3D problem in a set of 1D scalar equation arbitrarily oriented in space. The system of equations has been solved referring to a relative rotating framework for the moving components, whereas to an absolute reference elsewhere. The domain has been discretized on a basis of a polar coordinate system, identifying five macro sub-domains, namely the inlet pipe, impeller, vaneless diffuser, volute, outlet pipe, each treated numerically in a specific way. The diffuser's momentum in the tangential direction has been modelled resorting to the conservation of the angular momentum, while the rotor channels are modelled as rotating pipes that exchange work and momentum with the blades as they experience a relative source term due to the centrifugal force field and its potential. The model has been validated against measurements carried out on a steady state flow test bench at University of Genoa.

INTRODUCTION

The recent trend towards engine downsizing, followed in the last decade, has increased the adoption of charge boosting techniques to keep the engine performance at a competitive level, while reducing the fuel consumption. In the field of SI engines, this technique, combined with direct injection and advanced control of valve timing and lifts can represent a breakthrough technology towards the reduction of CO_2 emissions, making this propulsion system competitive with the state of the art of Diesel engines.

This scenario is particularly favorable to the adoption of modelling techniques, since the matching of the turbocharger and the variable actuation of valves along with the need of achieving a suitable level of temperature for the after-treatment system, requires a careful tuning of all the engine parameters. This can be achieved resorting to 0D or 1D models, specifically developed for the simulation of internal combustion engines [1], rather than with the adoption of complex 3D CFD tools [2], which may result too demanding in terms of computational resources and computation time. From a modelling point of view, the simulation of turbocharging devices has always been a challenge in the field of CFD: the compressibility phenomena, along with the occurrence of supersonic flows, and the fluid dynamic instabilities that may arise when they run in off design condition are the major difficulties that engineers can encounter during their simulation. At research level CFD offers detailed methods to capture the incipient stall and surge based on RANS and LES approaches [3] to deeply understand the behavior of these machines. These methods, however, are too detailed and demanding, form a computational point of view, that they

can hardly be used for industrial purposes, especially if DOE or iterative procedures must be adopted to achieve the optimum engine calibration. At engine calibration level, 0D and 1D models are usually preferred, since they are flexible, robust and quick. They rely on the usage of predefined maps of the turbocharger which are accessed runtime in the code to calculate intra pipe boundary conditions [4]. Several examples are available in the literature, where different approaches for the treatment of maps (pre-processing or interpolation) are described [5]. All of them have in common the usage of maps (for compressor or for turbine) that have been measured on steady state flow bench. Because of this, although useful for the modeling of engine configurations, they cannot be considered fully predictive. For instance, operating conditions that fall between two different characteristic lines (at different revolution speeds) are treated resorting to interpolation techniques between the two nearest curves. Some authors resort to 3D CFD to determine the compressor map with the desired refinement of isovelocity curves [6]. A solution to this problem has been proposed by [7] where a predictive 1D has been proposed as a mapless method. This approach is based on the modelling, under the 1D assumption, of rotating and stationary components, such as the impeller and the volute (plus eventual diffuser) in which source terms are added to the conservation equations to consider the effect of the centrifugal force field.

METHODOLOGY

The 3Dcell approach adopted in this work consist of reproducing the 3D geometry as a network of 0D elements, called cells (volumes), connected with each other by means of interface elements, called connectors or ports.
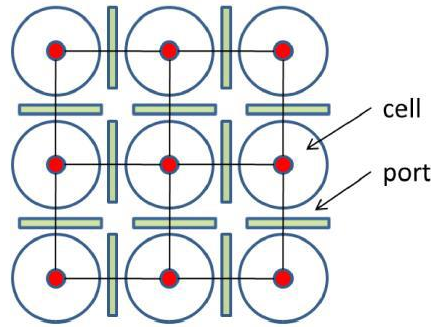

FIGURE 1. Example of cells and ports network

The quasi-3D domain is defined by means of two fundamental elements: the cell and the port. The cell element is defined by its volume and by the list of the connectors linked to it. The connector element stores information about the connectivity between neighboring cells, and geometrical parameter such as the distance from the adjacent cell centers, the direction with respect to an absolute orientation system and the flow area. Additional information stored in cells and ports may appear for every specific case, where quantities different form the standard ones must be defined (i.e. simple fluid cell, wall port). The main characteristic of 3Dcell is that the CFD simulation on a three-dimensional geometry reduces to a system of 1D problems along the direction of the normal of the ports surfaces, that carry the vectorial properties. [12]

The 3Dcell model is based on the formulation of the conservation equations of mass, momentum and energy for unsteady and compressible flows. Although they derive from the Navier-Stokes equations, in the actual context inviscid flow assumption is used, neglecting the second order partial derivative terms of the equation. Also, the effect of thermal diffusivity has not been considered. These approximations are acceptable for highly turbulent flow regimes where the inertial effects are prevailing over the viscous ones and when convection prevails against diffusion, leading in this way to the Euler set of equations:

$$\frac{\partial \rho}{\partial t} + \nabla \cdot (\rho \vec{v}) = 0 \quad \text{(conservation of mass)} \tag{1}$$

$$\frac{\partial (\rho e)}{\partial t} + \nabla \cdot (\rho h \vec{v}) = S_E \quad \text{(conservation of energy)} \tag{2}$$

$$\frac{\partial (\rho \vec{v})}{\partial t} + \nabla \cdot (\rho \vec{v} \vec{v}) = -\vec{\nabla} p + \vec{F} + S_M \quad \text{(conservation of momentum)} \tag{3}$$

The set of PDEs is then closed with the equation of state of perfect gas, $p = \rho R^* T$, which links, considering the compressibility, the density to pressure and temperature of the gas.

The solution procedure adopted by the numerical scheme is the explicit time marching, staggered leapfrog method, which means that fluxes at the ports are computed in an intermediate grid step both in time and space. Therefore, three different time levels are defined (t, t+1/2 and t+1) over which the three conservation equations are suitably defined. The pseudo-staggered arrangement in space and the explicit time marching staggered leapfrog method in time lead the 3Dcell to be second order accurate in both space and time.

As said, the numerical method allows a convenient discretization of the domain to decompose the generic three-dimensional problem in a set of much simpler 1-D equations along the normal of the ports. In fact, calling $v_n = \vec{v} \cdot \vec{n}_{port}$ the scalar product between the vectorial velocity crossing the connector and its normal direction, the vectorial problem can be solved by a system of scalar equations oriented in space as the normal itself. Denoting with subscripts L and R, the properties of the left and right cells connected to the oriented port, by expressing the flux terms as surface integrals, and exploiting the Gauss theorem, the integration of the momentum equation (3) over the control volume $A\Delta L$ leads to the following equation:

$$(\rho \vec{v} A)_{port}^{t+\frac{1}{2}} = (\rho \vec{v} A)_{port}^{t-\frac{1}{2}} + \frac{\Delta t}{\Delta L} A_{port}[(p + \rho v_n^2)_L^t - (p + \rho v_n^2)_R^t] - p^* \frac{dA_{port}}{dx} \pm S_M \,, \tag{4}$$

where A_{port} is the area of the port, ΔL is the distance between the connector and the cells centers, S_M is a generic source term of momentum (e.g. friction losses), and the term $\left(-p^* \frac{dA_{port}}{dx}\right)$ accounts for the variation in cross section area dA_{port} with p^* being the cell's pressure where the difference occurs and along the space coordinate dx.
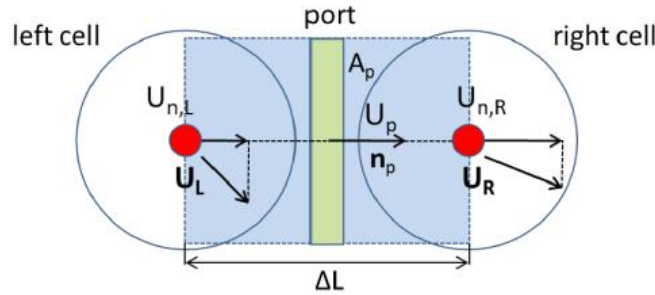
FIGURE 2. Control volume of momentum equation, showing the scalar decomposition of the velocity vector

Similarly, the continuity equation, integrated over a cell's volume is given by:

$$\rho_{cell}^{t+1} = \rho_{cell}^t + \frac{1}{V} \sum_{p=1}^{N_{ports}} (\rho v A)_p^{t+\frac{1}{2}} \Delta t \,, \tag{5}$$

where the surface integral, because of the discretization described above, resolves in a summation of the mass flows through the ports linked to the cell (N_{ports}). Note that the mass flows are directly derived from the momentum equations (4) with a positive or negative net contribution depending on whether entering or exiting the cell's control volume.

By considering the energy flux rather than the mass flux, and by adding the generic source term S_E, it is possible to write explicitly the energy equation in the cells:

$$(\rho e^0)_{cell}^{t+1} = (\rho e^0)_{cell}^t + \frac{1}{V} \sum_{p=1}^{N_{ports}} (\rho v h^0 A)_p^{t+\frac{1}{2}} \Delta t \pm S_E \,, \tag{6}$$

where e^0 is the total energy and $h^0 = e^0 + p/\rho$ is the total enthalpy.

The enthalpy at the port is evaluated by means of an upwind scheme, thus being $h^0 = h^0_{Lcell}$ if the mass flow comes from the left cell and $h^0 = h^0_{Rcell}$ otherwise. This kind of approach is preferred than linear interpolation since the advantages in gaining stability prevail against the need of achieving high accuracy.

According to the definition of pseudo-staggered arrangement [13], to allow the calculation of cell properties, the velocity must be defined also in the centroid of the cell element. For this purpose the cell momentum $(\rho \vec{v} V)_{cell}$ has been defined vectorially by the weighted average of the momentums of all the port linked to the cell, where their distance from the cell center has been used as weighting factor:

$$(\rho \vec{v} V)_{cell} = \sum_{p=1}^{N_{ports}} (\rho \vec{v} A)_p \Delta L_p .$$ (7)

The cell velocity vector is then determined from the cell momentum and from the mass of fluid contained in the cell.

Finally, the 3Dcell method is stabilized by adding a diffusion term to the momentum equation (hence the name DTM). From one side this practice dumps numerical oscillation but, on the other side, it causes the solution to be more numerically diffusive. Thus, since 3Dcell has been conceived as an acoustic simulation tool, in which the loss of accuracy cannot be accepted, DTM is applied with major strength locally, where the solution does not satisfy the boundedness propriety, i.e. where pressure discontinuities are present as discussed in [9].

The 3Dcel framework here presented has been adapted to model the fluid dynamics of turbomachines. In particular, in this work we will focus on the modelling of the compressor of an automotive turbocompressor. To this purpose the energy and momentum balances of ports and cells have been adapted to include specific source terms due to the presence of stationary and rotating components.

THE COMPRESSOR MODEL

The domain of the compressor has been discretized in cells and ports based on a polar coordinate system. This kind of discretization is convenient for at least two main reasons: it allows for a decomposition of the flows in its main radial and tangential directions, and, secondly, it makes straightforward to account for the change in position of the spatial meshes due to the impeller's rotation.
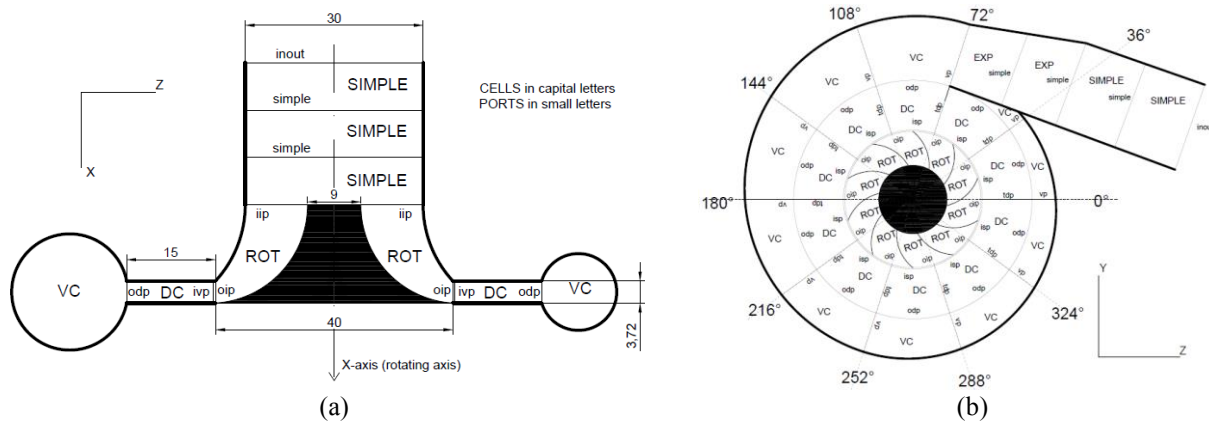
FIGURE 3. views of the axial (a) and meridian (b) plane of the discretized domain. Cells for the modelling of rotor, inlet, diffuser and volute are highlighted. Ports are located at the interface between the cells.

The compressor has been divided into five different regions; each one is treated numerically in a different way:
- The inlet region: where the flow is taken from a generic reservoir, or from an external 1D domain suitably coupled, and then distributed to the different channels of the impeller. In this region the flow is assumed to be monodimensional, since each cell (simple cell) is coupled to only two ports, and only one main direction is present.

- The impeller region: where the fluid exchanges work with the rotating blades. Also in this region, although the flow is being deflected, the assumption of 1D flow holds.

- The vaneless diffuser: where the pressure recovery occurs thanks to the increase of the flow section in the radial direction. In this region cells confine only with other fluid cells, and the flow is dominated by a free vortex pattern.

- The volute: usually with circular section and placed around the diffuser. Its cross section is growing along the tangential coordinate, as it collects the compressed air and delivers it to the outlet pipe.

- The outlet pipe: collects the air coming from the volute, and delivers it to the next element of the scheme. Here the flow returns to be one dimensional and it can be expanded if the cross section increases.

Model of the impeller

The impeller is discretized as an ensemble of independent rotating pipes. Each channel is discretized by a single cell (identified as ROT) whose connected ports, namely the inlet impeller port (IIP) and the outlet impeller port (OIP), have the same orientation of the corresponding blade angles. In this region the choice made is to refer to a relative reference framework, naturally accounting for the fact that the elements are rotating with the impeller. In this way the relative velocity will be given by the following vectorial equation:

$$\vec{w} = \vec{v} - \vec{u},\qquad(8)$$

where $\vec{u} = \vec{\omega} \times \vec{r}$ is the local peripheral velocity, and $\vec{v}$ the air velocity in the absolute reference system.

The momentum equation (4) for the impeller ports must be adjusted to account for the rotating framework. In particular, the momentum of the left and right cells must be referred to the relative frame through equation (8). This means that no actions are needed for the rotating cell, since its velocity is already the relative one, but for the inlet and outlet cells (that are fixed) the momentum must take into account the peripheral velocity. Being part of a rotating relative system, a centrifugal force field term must be added to the momentum equation:

$$\vec{F}_c = -\rho\left(\vec{\omega} \times (\vec{\omega} \times \vec{r})\right).\qquad(9)$$

Therefore, the momentum equation for the rotating ports can be written as follows:

$$(\rho\vec{w}A)_{port}^{t+\frac{1}{2}} = (\rho\vec{w}A)_{port}^{t-\frac{1}{2}} + \frac{\Delta t}{\Delta L}A_{port}[(p + \rho w_n^2)_L^t - (p + \rho w_n^2)_R^t] - p^*\frac{dA_{port}}{dx} + \left(\vec{F_c} \cdot \vec{n}\right)A_{port}.\qquad(10)$$

The inlet impeller ports are all connected to the last cell of the inlet pipe, sharing the same inlet properties. In particular, it can be noted, referring to Fig. 3a, how the inlet pipe is discretized resorting to a 1D strategy. A different situation occurs in the outlet impeller ports, that, due to their rotation, are connected with different regions of the vaneless diffuser, see Fig. 3b. For these ports there is not a fixed one to one connection with the diffuser cells, and the downstream properties are taken proportional to the overlapped area between stator and rotor cells as the latter rotates.

Similarly to what has been done to derive equation (10), also the generic energy equation (6) must be adjusted to fit a rotating reference frame. At the interface between stator and rotor, only static scalar properties are equal in value, and not the total ones, that are required by the method. In fact, passing from the absolute to the relative frame, the kinetic contributions of the total properties differ by the contribution of the peripheral velocity. For this reason, the total enthalpy in the ports is build up from the sum of the static enthalpy h^s of the downstream cell plus the relative kinetic energy of the port $w_p^2/2$. Moreover, the cell is exchanging work with the blades, and this represents a net source term in the conservation equation. The adjusted equation can be written as:

$$(\rho e^0)_{cell}^{t+1} = (\rho e^0)_{cell}^t + \frac{1}{V}\sum_{p=1}^{Nports}\left(\rho w(h^s + \frac{w^2}{2})A\right)_p^{t+\frac{1}{2}}\Delta t + \Delta t\left[\left(\rho w A\frac{u^2}{2}\right)_{oip} - \left(\rho w A\frac{u^2}{2}\right)_{iip}\right].\qquad(11)$$

Diffuser and volute model

In the diffuser region, the solution of the momentum conservation equations is solved referring to the absolute reference system and contains only the wall friction source term. The flow in this region should guarantee the conservation of the angular momentum. Hence, the tangential component of the absolute velocity is also assigned to the port belonging to the vaneless diffuser, instead of only the component directed as the port normal. This results in the solution of two equations:

- the momentum conservation along the radial direction

$$(\rho \vec{v}_{rad} A)_{port}^{t+\frac{1}{2}} = (\rho \vec{v}_{rad} A)_{port}^{t-\frac{1}{2}} + \frac{\Delta t}{\Delta L} A_{port}[(p + \rho v_{rad}^2)_L^t - (p + \rho v_{rad}^2)_R^t] + S_{friction}, \tag{12}$$

- the free vortex equation

$$v_{tang} \cdot r = constant. \tag{13}$$

As what concerns the volute and outlet pipe, the solution of continuity, energy and momentum equations require no particular treatment, as in these regions, equations (4), (5) and (6) hold.

Distributed friction losses

The presence of friction is the main source of distributed losses. In this approach they have been taken into account with the term S_M, which appears as a negative contribution in momentum equation (4). This source term is function of the mass flow rate as follows:

$$F = (\rho \vec{v} A)_{port}^{t+\frac{1}{2}} |\vec{v}_{port}| f_{coeff} \frac{2}{d_{h,port}}, \tag{14}$$

where f_{coeff} is the friction coefficient, that for a fully developed turbulent flow can be assumed as constant, and $d_{h,port}$ is the equivalent diameter of the port i.e. the diameter of a port with same cross-sectional area but with circular shape:

$$d_{h,port} = \sqrt{\frac{4 \cdot A_{port}}{\pi}}. \tag{15}$$

Slip factor

In radial turbomachinery, the slip factor is a measure of the fluid slip in the impeller of a compressor. This slip is the deviation, quantified as the angle at which the fluid leaves the impeller with respect to the impeller's blade/vane angle. It is an important phenomenon and in radial impellers it affects the transfer of work between the fluid and the machine, since it changes the velocity triangles. To mimic the effect of the slip, Stanitz's equation has been introduced, where the slip velocity is assumed to depend upon of the blade exit angle according to the following equation:

$$\sigma = 1 - \frac{1.98}{z\left(1 - \frac{v_{2,rad}}{u_2} cotg\beta_2\right)}, \tag{16}$$
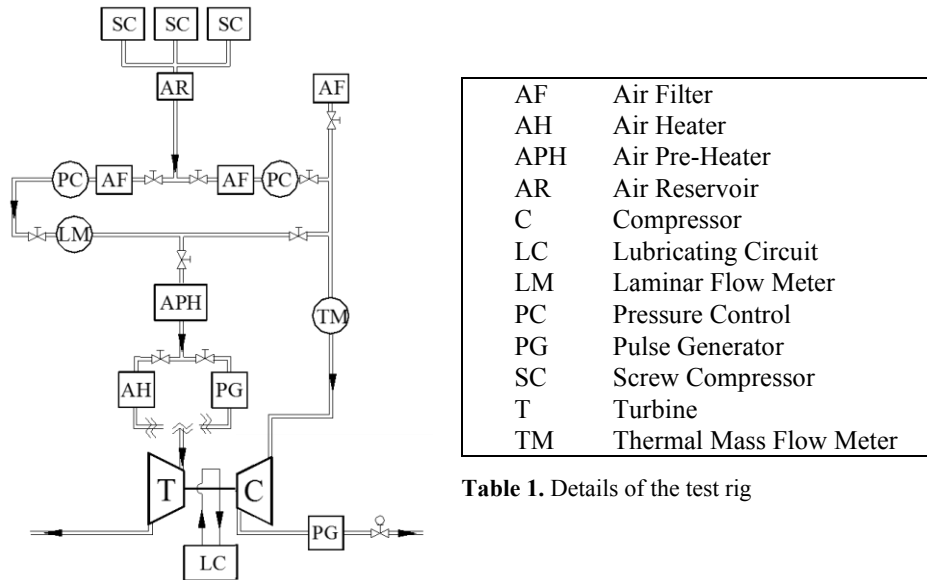
where, Z is the number of blades, β_2 varies from 90 to 135 and σ is the ratio between the real and ideal projection of the relative velocity w along the direction of the peripheral velocity.

This correlation is adopted to determine the new tangential component of w and v and therefore to correct the amount of work exchanged between the blades and the fluid.

EXPERIMENTAL SET-UP

The experimental activity was performed on a small turbocharger compressor (with an impeller outlet diameter of 40 mm) used for a downsized Spark Ignition automotive engine. Compressor steady flow maps were measured on the test facility operating at the University of Genoa. This rig, schematically shown in Fig. 4, consists of a compressed-air equipment that allows to perform investigations on intake and exhaust automotive components both under steady and unsteady flow conditions [11].

AF	Air Filter
AH	Air Heater
APH	Air Pre-Heater
AR	Air Reservoir
C	Compressor
LC	Lubricating Circuit
LM	Laminar Flow Meter
PC	Pressure Control
PG	Pulse Generator
SC	Screw Compressor
T	Turbine
TM	Thermal Mass Flow Meter

Table 1. Details of the test rig

FIGURE 4. Schematic layout of the turbocharger test facility of the University of Genoa

Three screw compressors supply a total mass flow rate of 0.6 kg/s at a maximum pressure of 8 bar. The test rig is particularly suitable to test automotive turbochargers thanks to the availability of two independent feeding lines. Experimental investigations can be performed under "cold" and "hot" conditions by properly modulating the thermal power of an electric air heating device that permits to heat turbine inlet air up to 750 °C, depending on the size of tested component. The facility set-up is very convenient in particular to conduct tests on automotive turbochargers and to study performances of only one of the two machines without the need of disassembling the whole system but regulating air conditions at the inlet of the turbine and of the compressor. When testing the working conditions of the compressor, the turbine is used as the driver machine varying the flows conditions to obtain the operating points needed by the compressor, the power absorbed by the compressor plus power lost in the bearing system. When testing the turbine, the compressor is used as a brake in order to change the absorbed power and change the compressor operating point.

An automatic data acquisition system allows to gather measurements of thermodynamic parameters at different measuring sections. Three different pressure wall taps and three temperature probes (circumferentially located at 120°) are used in order to evaluate the compressor efficiency. Strain-gauge and piezoresistive transducers characterized by an accuracy of ±0.15% of the full scale are employed to measure static pressures. Air temperatures are measured through platinum resistance thermometers (Pt 100 Ohm, accuracy of ± 0.15 °C + 0.2% of measured value). The turbocharger rotational speed is estimated using an eddy current probe mounted close to the compressor wheel with an accuracy of ±0.009% of full scale. A thermal mass flow meter is used to measure compressor mass flow rate with an accuracy of ±0.9% of measured value and ±0.05% of the full scale.

The compressor measured at the test bench and modelled via the quasi-3D approach is an IHI-RHF3 whose main specifications are summarized in Table 2.

Compressor steady flow characteristics curves were measured referring to the following parameters:

corrected rotational speed: $n_{cr} = \frac{n\sqrt{T_0}}{\sqrt{T_{T1}}}$ [rpm]

total-to-total compression ratio: $\beta_{cTT} = \frac{p_{T2}}{p_{T1}}$ [-]

corrected mass flow rate: $M_{cr} = \frac{M_c p_0 \sqrt{T_{T1}}}{p_{T1}\sqrt{T_0}}$ [kg/s]

total-to-total isentropic efficiency: $\eta_{cTT} = \frac{T_{T2is}-T_{T1}}{T_{T2}-T_{T1}}$ [-]

|	
Number of impeller channels	10
Diameter of the compressor hub at the outlet	0.04 m
Height of the compressor	0.0165 m
Diameter of compressor hub at the inlet	0.009 m
Inlet blade angle (for all three impeller)	110°
Blade height at the outlet	0.003722 m
Impeller outlet blade angle	135°
Length of the vaneless diffuser	0.015 m
Height of the vaneless diffuser	0.003722 m

Table 2. Compressor's main geometrical parameters

where T_{T1}, p_{T1} are compressor inlet total temperature and pressure and p_{T1}, T_{T2} and T_{T2is} are the compressor outlet total properties of pressure, temperature and temperature for an isentropic expansion for the same β_{cTT}.

The reference temperature and pressure have been chosen as T_0= 293.15 K, p_0= 0.980 bar.

RESULTS

The described quasi-3D model can be used as a standalone solver if coupled with simple boundary conditions, like a reservoir, an isentropic inlet, or an open end. Nevertheless, for this study, the code has been included in the thermo-fluid dynamic simulation software gasdyn, that allows the replication of a wider range of boundary conditions. In particular, at the compressor inlet, a mass flow at a constant temperature has been imposed, whose pressure depends on the backpressure generated by the rotating machinery and by the open end downstream. Varying the mass flow entering the compressor, as well as its rotating speed, it has been possible to generate the performance maps as function of the corrected mass. The results obtained by the code have been then validated against the measured data provided by University of Genoa.
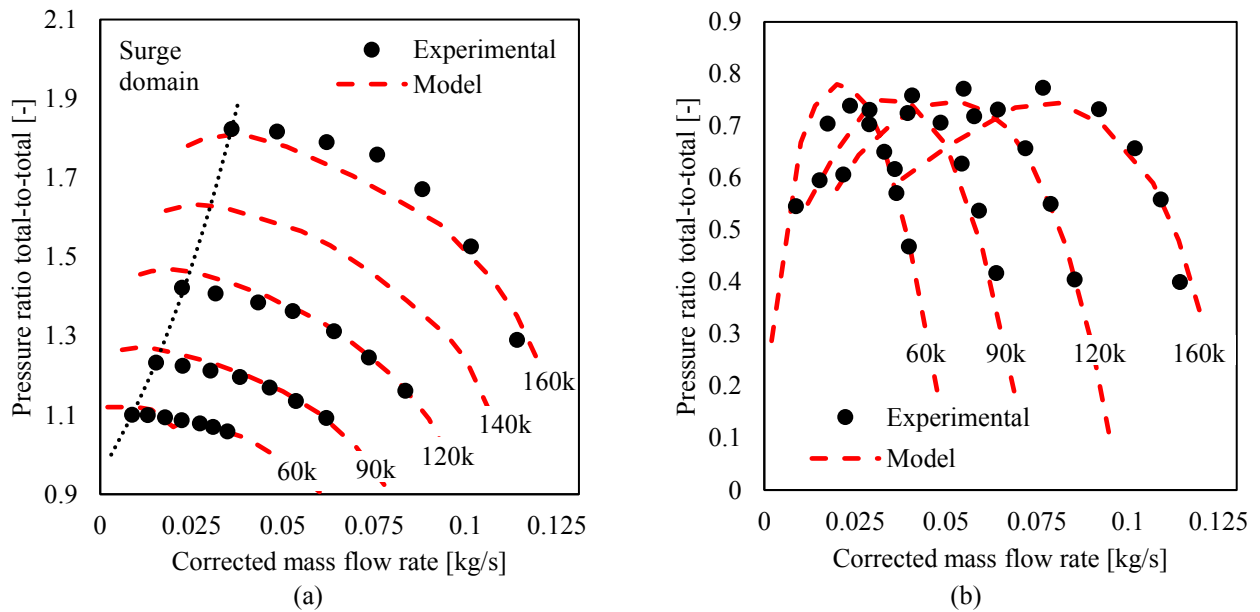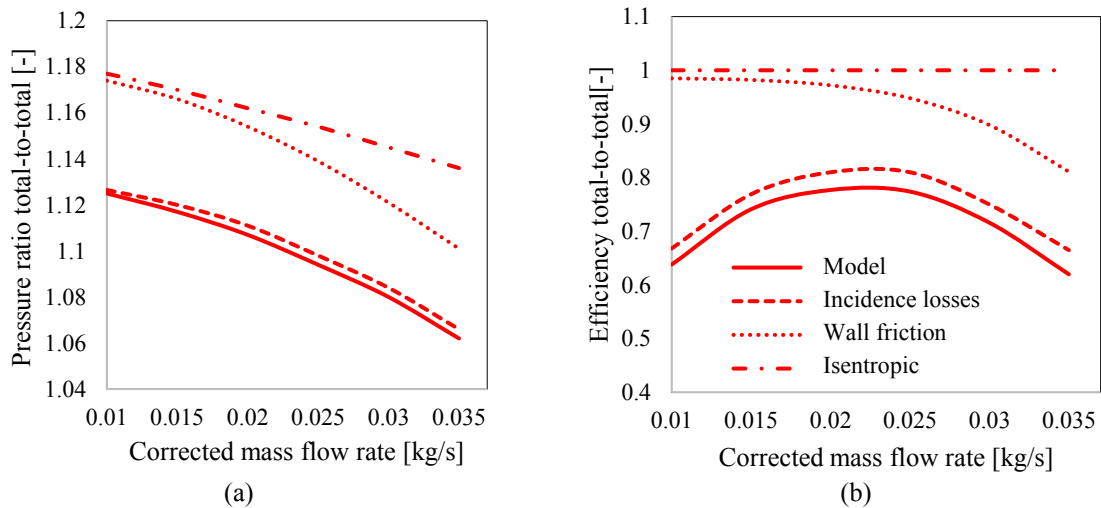

FIGURE 5. (a) total to total pressure ratio and (b) total to total efficiency as function of the corrected mass flow: comparison between experimental values and calculated ones for rotation speed from 60k rpm to 160k rpm

Figure 5 shows the results of the simulation campaign, where the total to total compression ratio and the total-to-total efficiency, plotted versus the corrected mass flow rate, are compared to those provided by the experimental measurements. The model is proved to be capable of predicting the compressor's performances at different iso-velocities ranging from 60000 RPM to 160000 RPM (1000 to 2670 RPS).

The compression ratio, Fig. 5a, is correctly evaluated for all the flow rates investigated, but slightly over-estimated for the lowest ones. However, it has to be pointed out that not all the phenomena occurring in a real turbomachine have been modelled at this stage of the study. For example, tip blade leakage losses, are not included yet. This type of loss has a major influence at high delivery pressure when the leakage has a higher impact due to the higher density of the fluid and translates in a lower pressure ratio at little flows. A further aspect that can be the source of a mismatch, is the adiabaticity assumption of the model. While it is certainly true for the simulation, this cannot be guaranteed during the measurements and therefore can cause a deviation between the two curves.

The model was also capable to extend the map leftwards in the surge zone, in which the compression ratios are decreasing, leading to the typical fluid-dynamic instabilities. Similarly, the map was extended rightwards in the choke domain, where the iso-velocity curves experience a steep decrease in delivery pressure for increasing flow rates, as compressibility effects become more and more important.

The total to total efficiency, shown in Fig. 5b, reproduces the typical bell shape of the iso-rotation curves with the ascending and decreasing sections fitting fairly well the experimental values, while the maximum points are slightly decreasing as the rotation increase, instead of remaining constant. As for the compression ratio, this behaviour could be linked to the imperfect adiabaticity of the experimental results, considered that the maximum deviations in absolute value of temperature are lower than 0.5°C for the curve at 60k rpm, and 2°C at 160k rpm, compared with increment in temperature in the range of 10°C and 65°C, respectively.

(a)   (b)

FIGURE 6. (a) total to total pressure ratio and (b) total to total efficiency as function of the corrected mass flow: effect of friction, inlet blade incidence and slip losses at 60k rpm.

In Fig. 6 the effect of three of the main losses, namely friction, inlet blade incidence, and slip losses, is shown. The dash dotted lines are the ideal curves: the compression ratio is decreasing for higher flow rates, as we were expecting from a backswept impeller, and the efficiency is a flat curve at 1, being representative of an isentropic process. The gas wall friction loss effects, showed by the dotted lines, are proportional to the square of the flow's velocity, as described in equation (14), and their contribution grows as the mass flow increases. Summing up the incidence losses we obtain the dashed curve. For this set-up this kind of losses are very important, especially at low flow rates, since the difference of the flow's relative direction entering the impeller is far from the blade orientation. The incidence losses are included in the model in a natural way. In fact, the momentum of the inlet ports (as well as in all ports) is evaluated considering only the contributions that are normal to the ports themselves. The last type of losses considered in this analysis are the slip losses. These losses take place at the impeller outlet as the physical consequence of the gradients that establish between the suction side and pressure side of the blades.

CONCLUSIONS

In this work a quasi3D approach, namely the 3Dcell, for the modelling of radial compressor dedicated to the supercharging of internal combustion engines has been presented. Originally this approach was conceived for the acoustic simulation of complex 3D shapes, but it has been adapted to the fluid dynamic simulation of engine components. In this work, the rotation of components and the evaluation of the momentum and energy transfer has been included in the conservation equations. The rotating component is suitably interfaced with the stationary part of the compressor, allowing to capture the effects due to the blade passage. The discretization of the equation follows the staggered grid assumption and considers both relative or absolute velocity when the rotor or the volute are addressed, respectively. The space domain discretization is based on the construction of a network of 0D and 1D elements, namely the cells and the ports. In particular, only one cell and two ports (one for the inlet and one for the outlet the impeller) have been used to discretize the blade channel. The volute is constructed with a one to one cell ratio in the circumferential direction with the rotor. This results in an extremely light mesh size, favorable for the reduction of the computation runtime. The quasi3D model has been coupled with the 1D code Gasdyn and used to reproduce stationary test bench results. It has been proved that the model is capable of predicting the delivery pressure measured at a compressor test bench at different mass flow rates and revolution speed with a fairly good agreement also in terms of efficiency prediction. This means that the approach can be used for a mapless simulation of and internal combustion engine equipped with a turbocharger, since the model is able to derive the compressor maps by itself.

REFERENCES

1.   Onorati, A., Ferrari, G., D'Errico, G., Montenegro, G. The prediction of 1D unsteady flows in the exhaust system of a S.I. Engine including chemical reactions in the gas and solid phase (2002), 2002-01-0003, SAE Technical Papers,
2.   Trigui, N., Griaznov, V., Affes, H., Smith, D. CFD based shape optimization of IC engine (1999) Revue de l'Institute Francais du Petrole, 54 (2), pp. 297-307
3.   Semlitsch, B., Mihăescu, M. Flow phenomena leading to surge in a centrifugal compressor (2016) Energy, 103, pp. 572-587
4.   D. E. Winterbone and R. J. Pearson. Theory of engine manifold design. Professional Engineering Publishing, London, 2000.
5.   Galindo, J., Arnau, F.J., Tiseira, A., Piqueras, P. Solution of the turbocompressor boundary condition for one-dimensional gas-dynamic codes (2010) Mathematical and Computer Modelling, 52 (7-8), pp. 1288-1297
6.   D'Errico, G., Montenegro, G., Onorati, A., Merola, S., Vaglieco, B.M. Thermo-fluid dynamic modeling and experimental investigation of a turbocharged common rail di diesel engine (2005) SAE Technical Papers, 2005-01-0689
7.   De Bellis, V., Bozza, F., Bevilacqua, M., Bonamassa, G., Schernus, C. Validation of a 1D Compressor Model for Performance Prediction (2013) SAE International Journal of Engines, 6 (3), pp. 1786-1800.
8.   Montenegro, G., Della Torre, A., Onorati, A., Fairbrother, R. A nonlinear Quasi-3D approach for the modeling of mufflers with perforated elements and sound-absorbing material (2013) Advances in Acoustics and Vibration, art. no. 546120.
9.   Montenegro, G., Onorati, A., Cerri, T., Della Torre, A. A quasi-3D model for the simulation of the unsteady flows in I.C. engine pipe systems (2012) SAE Technical Papers 2012-01-0675
10.   H.K. Versteeg and W. Malalasekera. An Introduction to Computational Fluid Dynamics: The Finite Volume Method, volume Vol. I. Pearson Education Ltd., Harlow, Essex, UK, 2007.
11.   Marelli S., Marmorato G., Capobianco M., Evaluation of heat transfer effects in small turbochargers by theoretical model and its experimental validation, Energy, Elsevier, 2016, doi:10.1016/j.energy.2016.06.067.
12.   Montenegro, G., Onorati, A., Piscaglia, F., D'Errico, G. Integrated 1D-MultiD fluid dynamic models for the simulation of I.C.E. Intake and exhaust systems (2007) SAE Technical Papers
13.   Torre, A.D., Montenegro, G., Cerri, T., Onorati, A. A 1D/Quasi-3D coupled model for the simulation of I.C. engines: Development and application of an automatic cell-network generator (2017) SAE International Journal of Engines, 10 (2), pp. 471-482.